Journal of Engineering Mathematics **42:** 243–253, 2002.

Numerical modeling of liquid withdrawal from gravure cavities in coating operations; the effect of cell pattern

LEONARD W. SCHWARTZ
University of Delaware, Department of Mechanical Engineering, Newark, DE 19716, USA

Received 19 September 2001; accepted in revised form 14 February 2002

Abstract. A particular free-surface flow of industrial importance is the unsteady motion of a thin layer of viscous liquid on an engraved solid surface or substrate. A model is presented and numerical studies are performed for the cell-emptying behaviour when an engraved roller is used to transfer a liquid coating onto a moving belt or web. The three-dimensional unsteady liquid motion is calculated where the flow domain is bounded above by a stress-free surface and bounded below by a moving substrate with one of several different patterns of indentations. The goal is to ascertain, theoretically, how the choice of pattern affects the performance of the substrate. The physical model is simplified through use of the long-wave or lubrication approximation that is appropriate to liquid flow in thin layers. Three different patterns of cells: square, diamond and hexagonal, are considered. In each case the cell shape is taken to be paraboloidal. Early-time cell emptying is found to be quite independent of pattern. There is a degree of re-filling however, which is pattern-dependent. In this work, a high degree of symmetry is exploited to reduce the size of the numerical computations. Only Newtonian liquids are considered.

Key words: gravure rollers, industrial coating, mathematical modeling, numerical simulation.

1. Introduction

A number of industrial processes involve the application of a thin liquid coating layer of a solution or suspension to a flexible sheet or 'web'. Often the purpose is to alter the surface characteristics of the web after the liquid has been removed by drying. Many desirable product characteristics may be imparted by the coating. These include, for example, antistatic properties, better ink adhesion for printing applications, and improved adhesion of vacuum-deposited metals to provide an oxygen barrier for food products. Typically it is necessary to minimize the variability of these surface characteristics. In practice, one must choose a coating process that is capable of applying the liquid to the specified level of uniformity.

A wide range of coating operations use rollers to apply the liquid film to the moving web. Many different methods of application exist ranging from single to multiple roll systems. For liquids of relatively low viscosity, a knurled or 'gravured' roller may be used, so called due to the large number of cells (typically 10's to 100's of microns in size) engraved throughout its surface. These cells retain liquid when the roll is removed from a bath or enclosed chamber of coating fluid; a proportion of this liquid is then given up to a rubber applicator roll (*e.g.* offset coating) or straight onto the web (direct gravure coating). Practical information on coating technology in general and roll or rotary coating in particular is given by Shepherd [1, Chapter 3].

A typical, albeit simplified, diagram of a rotary gravure coating operation is shown in Figure 1. Liquid is picked up from the bath B by the gravured roller GR. The roller radius is R and it is rotating at an angular speed ω. The knife blade, labeled K in the figure, may or

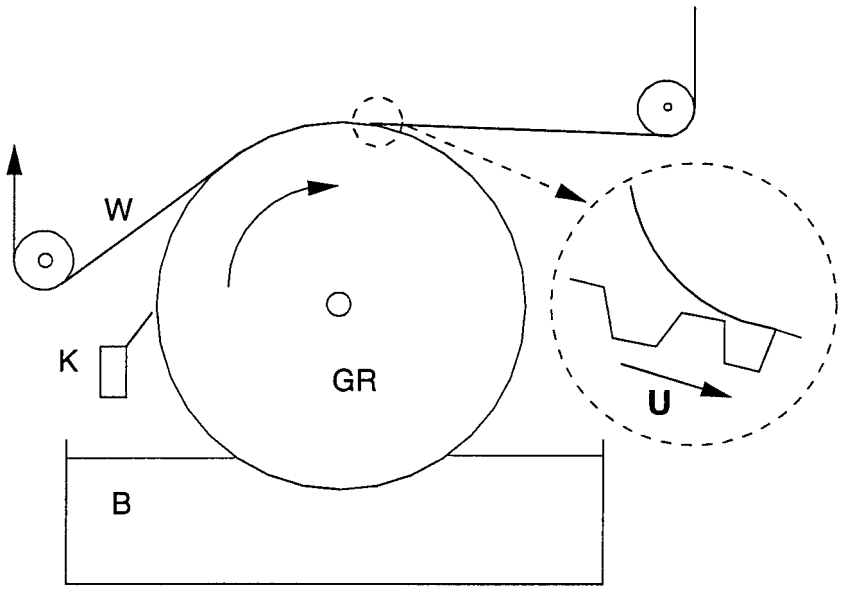

Figure 1. Schematic diagram of a roll coater that removes liquid from a bath B and transfers it to the moving web W. The small gravure cells are seen in enlargement in the inset where the liquid-air meniscus is also shown. This paper deals with flow in the liquid region bounded by the gravure and the mensicus.

may not be present. When it is there, it provides an absolute limitation to the coating thickness, since it is set at a fixed small distance from the roller. If the knife is not used, the amount of liquid that is picked up from the bath, and carried by the roller, is determined largely by the roller speed $U = \omega R$, the viscosity μ of the liquid, the liquid surface tension σ, and the acceleration of gravity g. For an ideally smooth roller rotating at sufficiently low speeds, the basic solution is given in the classical work of Landau and Levich. They treated the closely-related problem of determining the coating thickness on a flat plate that is removed vertically from a bath [2, pp. 674–683]. In their solution the ratio of the applied thickness H to the so-called capillary length $(\rho g/\sigma)^{1/2}$ is a function only of the capillary number $\mu U/\sigma$. Their solution was generalized by Wilson in several ways, including, in this context, the situation where the substrate is not perpendicular to the ambient fluid level in the bath [3]. This liquid flux is established in the small region where the rotating roller meets the bath.

Mass conservation dictates that the liquid flux onto the roller, under steady-state operating conditions, must be equal to the sum of the flux applied to the web and the flux returned to the bath. Determination of the flux returned to the bath is equivalent to the so-called *gravure-cell evacuation problem* for an engraved roller. We are concerned therefore with the amount of liquid remaining in the indentations or cells. As shown in the inset in Figure 1, this problem may be idealized by considering a moving sequence of cells under an almost steady liquid-air interface or *meniscus.*

In addition to being an important determinant of the coating-process efficiency, *i.e.* the liquid-coating thickness applied to the moving web, the cell-evacuation problem is also relevant to another aspect of gravure coating. Coating remaining in the cells leads eventually to a build-up of dried coating. When this build-up reaches a significant level, the ability of the gravure to function efficiently and pick up the necessary amount of liquid is impaired. At such times the continuous coating operation must be stopped, so that the gravure roller

may be replaced. The frequency of stoppage, because of gravure clogging, strongly impacts production efficiency.

Recently we have developed a numerical method, using the lubrication approximation, to calculate the three-dimensional unsteady flow during the gravure-cell emptying process [4]. In that work we considered only a square pattern of cells and found solutions for both Newtonian and shear-thinning coating liquids. The cell shape was taken to be a trapezoidal solid. Cell size was shown to be the principal determinant of emptying, with larger cells emptying more completely. A suitable nondimensionalization of the simplified governing equations, when the lubrication approximation is used, is all that is necessary to reach this conclusion. Gravure-cell dimensions are measured in units that vary directly with surface tension σ; thus it is clear that it is surface tension that is the principal cause of liquid retention in the cells. This is consistent with experimental observation [5]. More recent two-dimensional finite-element simulations confirm the importance of cell size in controlling emptying [6]. This would appear to suggest a simple solution: better cell emptying will be obtained simply by making the cell size larger. In practice, however, very large cells have been shown to cause problems with final coating uniformity and appearance. Overly large cells may also damage, *i.e.* scratch, the substrate or web.

Here we consider other cell patterns, but restrict consideration to cells of paraboloidal shape and Newtonian coating liquids. The pattern is specified with three parameters; these give the cell spacing in directions parallel and perpendicular to the roll, and the offset, parallel to the roll, of alternating rows of cells.

In the following section we discuss the evolution equation used in the simulation. New work on cell and pattern geometry is then presented. Section 3 deals with the computational procedure and discusses the results. Suggestions for further work are included in the final section.

2. The mathematical and numerical model

The inset in Figure 1 shows a gravured solid plate moving rightward with speed U under an essentially fixed liquid-air mensicus. The radius of the wheel GR varies in practice from several centimeters to a meter or more. It is very much larger than both the cell dimension and the radius of curvature of the meniscus. Thus, to a good approximation, we will ignore the gross curvature of the gravured surface.

We consider a pattern of indenture in two dimensions where x is taken in the direction of substrate motion. For definiteness, consider the gravure to consist of a planar 'land' with indentations. Take the land to be the (x, y) plane; thus the y direction is transverse to the gravure motion. The coordinate z measures displacement in the normal direction. The functions $z = h(x, y, t)$ and $z = h_1(x, y, t)$ represent the liquid free surface and the moving substrate respectively. The rigid substrate moves at constant speed U in the positive x direction; thus h_1 satisfies the equation

$$h_{1t} = -U\ h_{1x}, \tag{1a}$$

where subscripts signifiy partial derivatives and t is time. The total layer thickness $h_2 = h - h_1$ satisfies the lubrication evolution equation

$$h_{2t} = -\nabla \cdot \mathbf{Q}_2, \tag{1b}$$

where $\mathbf{Q}_2$ is the vector areal flow rate given by

$$\mathbf{Q}_2 = U h_2 \, \mathbf{i} - \frac{h_2^3}{3\mu} \nabla p. \tag{1c}$$

Here $\mathbf{i}$ is a unit vector in the x-direction. Equations (1a) and (1b) are both exact. The second of these is an integral statement of conservation of mass within the liquid region and $\mathbf{Q_2} = \mathbf{Q_2}(x, y, t)$. Equation (1c) uses the long-wave or lubrication approximation; this theory requires that the layer is sufficiently thin that the Reynolds number for the flow is small and also that the inclinations of both the free surface and the gravure, relative to the land, are nominally small as well. Thus the flow is 'slowly varying' along the substrate. Careful derivations of this approximation are give by Benney [7] and Atherton and Homsy [8] who extended the well-known Reynolds equation of lubrication theory to flows with free boundaries. A calculation of two-dimensional free-surface flow over a fixed substrate with indentations, and invoking the lubrication approximation, was given by Kim *et al.* [9]. A number of other specific applications of lubrication-type approximations to rotary coating have also appeared [10, 11].

The pressure gradient, under the lubrication approximation, is uniform across the thin dimension of the liquid coating; thus it is $p(x, y, t)$. It is given by

$$\nabla p = -\sigma \nabla \nabla^2 h, \tag{2}$$

where $\nabla^2 h$ is the small-slope approximation to the free-surface curvature. Adding Equations (1a) and (1b) we obtain the final evolution equation for the free surface,

$$h_t = -U h_x - \frac{\sigma}{3\mu} \nabla \cdot (h_2^3 \, \nabla \nabla^2 h). \tag{3}$$

Here σ is surface tension of the liquid coating and μ is the constant Newtonian viscosity. In obtaining these equations, we have applied the no-slip condition on the moving substrate and the condition of zero shear stress on the liquid surface.

Physical parameters can be removed from (2) by nondimensionalization. We take the gravure-cell depth h_0 as the length unit in which h and h_1 are measured; x and y are measured in units of the substrate length scale

$$L = h_0 \left(\frac{\sigma}{3\mu U} \right)^{1/3} \tag{4}$$

and the unit of time is

$$T^* = \frac{L}{U}. \tag{5}$$

In dimensionless units, the depth of gravure cells is one and the evolution equation is

$$\frac{\partial h}{\partial t} = -\frac{\partial h}{\partial x} - \nabla \cdot (s \nabla \nabla^2 h), \tag{6}$$

where $s = (h - h_1)^3$.

The dimensionless Equation (4) is solved by a finite-difference method in space and time. The substrate is discretized into an $M \times N$ rectangular computational domain. Spatial derivatives are approximated by use of central differences; thus the method is second-order accurate in space. Symmetry boundary conditions are imposed on three of the four sides, *i.e.*,

$$h_n = h_{nnn} = 0, \tag{7}$$

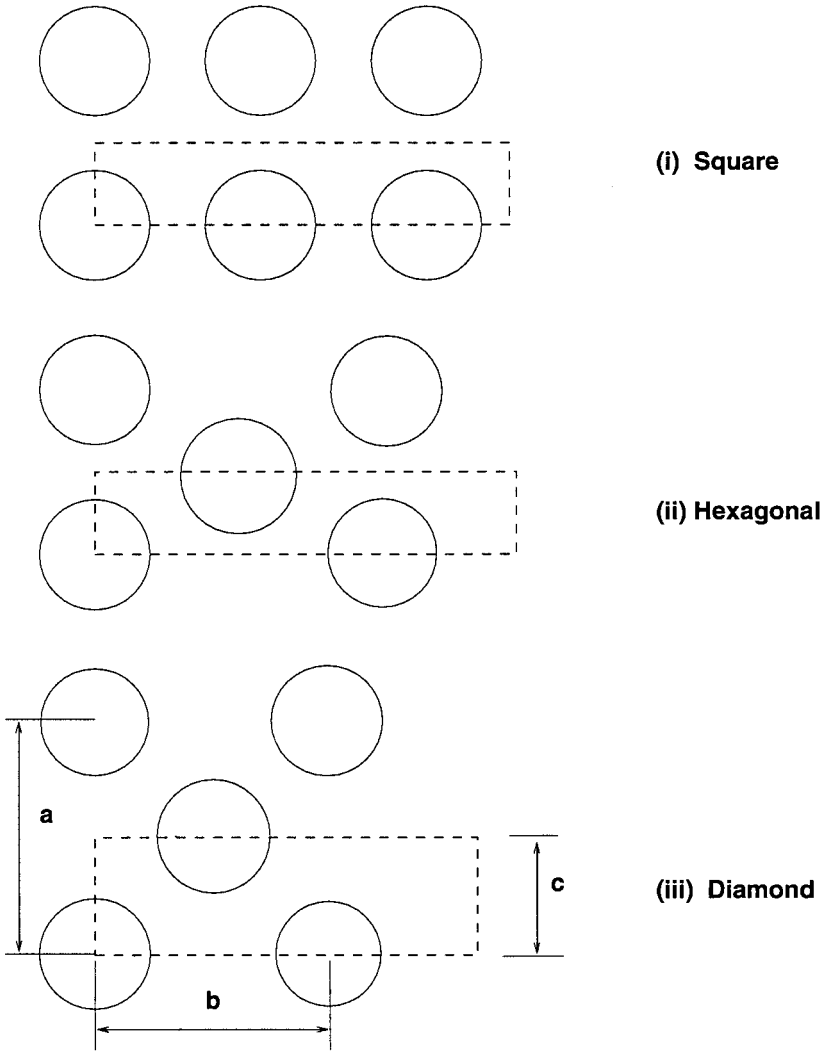

Figure 2. The three cell patterns considered. The dimensions a, b, c are input parameters. Because of symmetry, only a portion of the domains shown need to be calculated. Note that (iii) is the square pattern (i) rotated 45°.

where n is distance in the normal direction at each boundary. Time marching is made efficient by use of a semi-implicit method, as previously discussed [4, 11, 12]. The method is an extension of the well-known alternating-direction-implicit method, developed originally by Peaceman and coworkers [13], to the present fourth-order nonlinear field euqation. For a given simulation, computer usage is proportional to the number MN of calculated h values. Typical calculations require about one minute on a PC with a 500 Mhz processor, using the Linux operating system and a public-domain Fortran compiler. Surface profiles and contours are displayed dynamically during the calculation.

In each of the simulation results presented here, the free surface is pinned, for all y, at $(x, h) = (0, 5)$. The slope there is taken to be $h_{x0} = -6$ in dimensionless units. This slope specification is arbitrarily chosen; in a complete calculation of the flow, including the full gravure wheel and the web, its value would be found as part of the total solution. The slope value used here will be seen to illustrate the differences in behavior for the cell patterns

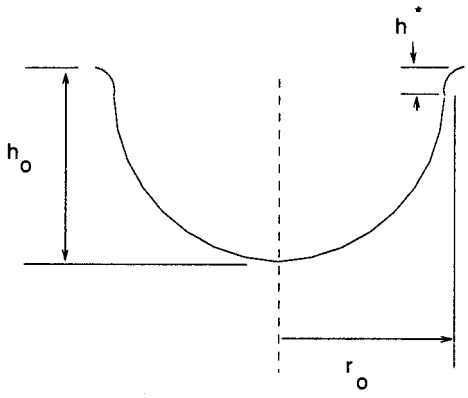

Figure 3. The paraboloidal gravure cell.

investigated. This slope condition gives cell-emptying values that are somewhat larger than those observed experimentally [5].

Starting with an initial exponential shape, we find that the liquid-surface variation becomes time-periodic after passage of about three cells. The computational window is fixed in space, while the gravure pattern moves at constant speed in the direction of x increasing. The 'steady-state' motion becomes periodic with a period equal to the cell-passage time, the time required for any given cell to move one wavelength downstream.

Unlike our previously reported work [4], maximum symmetry of the cell pattern is exploited here to minimize the amount of computation. A portion of the actual calculation 'window' is shown by the rectangles in the diagrams of Figure 2 where three cell patterns, termed (i) square, (ii) hexagonal, and (iii) diamond, are illustrated. As explained below, the calculation only needs to be performed over the small 'height' of each rectangle (*i.e.* in the cross-web direction). The offset per row, denoted c, is zero for the square pattern; it is equal to $a/2$ for the other two. Note that the diamond pattern, with $b = a$, is the square pattern turned 45° to the direction of web motion. Typically, the calculation window in the web motion direction is set to a length of $5b$.

The cells are currently taken to be paraboloidal, with a radius equal to r_0, except for a small 'fairing' at their upper edges as shown in Figure 3. This shape is similar to those used in many gravure applications. The cell profile has a continuous tangent and joins smoothly to the gravure land level. The cell shape is given by

$$h_1(r) = -h_0\left(1 - \frac{r^2}{r_0^2}\right), \quad r/r_0 \leq \sqrt{1 - h^*/h_0} \tag{8}$$

and

$$h_1(r) = -\frac{h_0^2}{h^*}\left(1 - \sqrt{1 - h^*/h_0}\ \frac{r}{r_0}\right)^2, \quad \sqrt{1 - h^*/h_0} < \frac{r}{r_0} < \frac{1}{\sqrt{1 - h^*/h_0}}. \tag{9}$$

The fairing height h^* is adjustable and a typical value is $0{\cdot}2h_0$. We can genralize the cell shape using other functions for $h_1(r)$.

A rendered plot of the gravure surface, specifically the computational 'window', is shown in Figure 4. The hexagonal pattern is illustrated. Reflection symmetry is imposed on the long boundaries; thus, the calculation only needs to be performed on the region shown. The dimensions of the computational array are $M = 30$ and $N = 260$ for the hexagonal pattern.

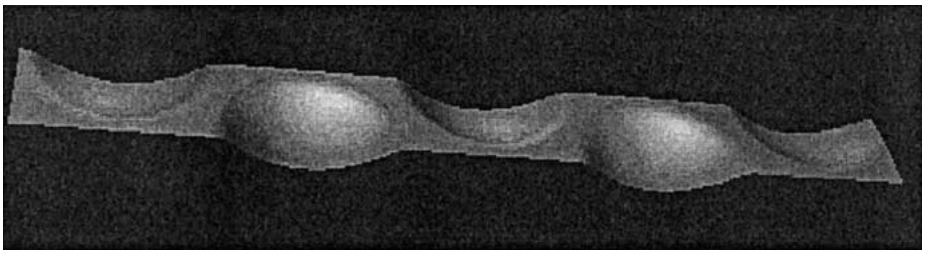

Figure 4. Rendered picture of the pattern of gravure indentations. Hexagonal pattern. This is the size of the computational domain that was used.

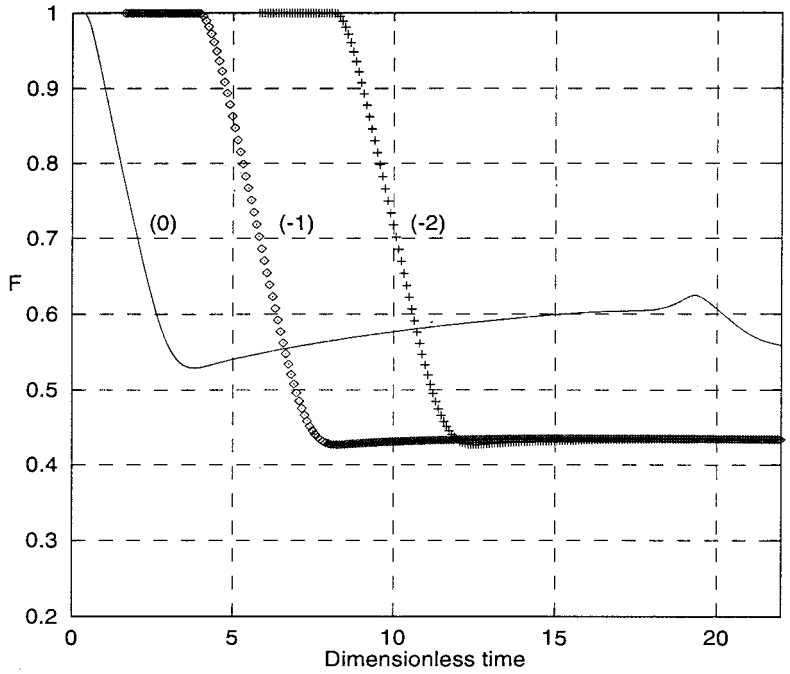

Figure 5. Cell fill fraction F vs. time for three identified cells, hexagonal pattern. The (0) cell lies at the origin $(x, y) = (0, 0)$ at time $t = 0$. Cells (-1) and (-2) lie in the following two rows, respectively.

3. Calculated results and discussion

There are a number of parameter combinations that determine the degree of cell emptying. In general, increasing the cell size and increasing the magnitude of the meniscus slope will both cause the cells to empty more completely. For the results shown here, we explore only the effect of the cell pattern. The parameter values used are $r_0 = 2{\cdot}5$, $h^* = 0{\cdot}2$, and $|h_{x0}| = 6$. The pattern and (a, b, c) values are (i) square: (6,6,3), (ii) hexagonal (6,5.2,3), (iii) diamond $(6\sqrt{2}, 6/\sqrt{2}, 6/\sqrt{2})$.

Figure 5 shows F, the fraction of cell volume filled with liquid, plotted *vs.* time, for the hexagonal pattern. Results for three cells are shown. Cell (0) starts directly under the meniscus; it is not completely 'processed' by the large pressure gradients in the meniscus region before it passes away as the substrate moves. Cells (-1) and (-2) are the next two cells that pass under the meniscus. The emptying behavior is seen to be the same for both; this indicates

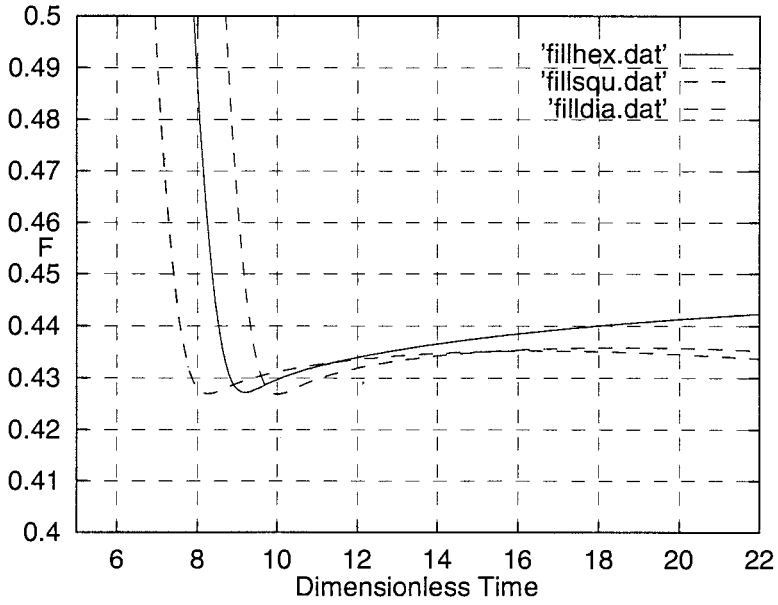

Figure 6. Cell fill fraction F vs. time. Three cell patterns are compared. For clarity, the scales have been expanded.

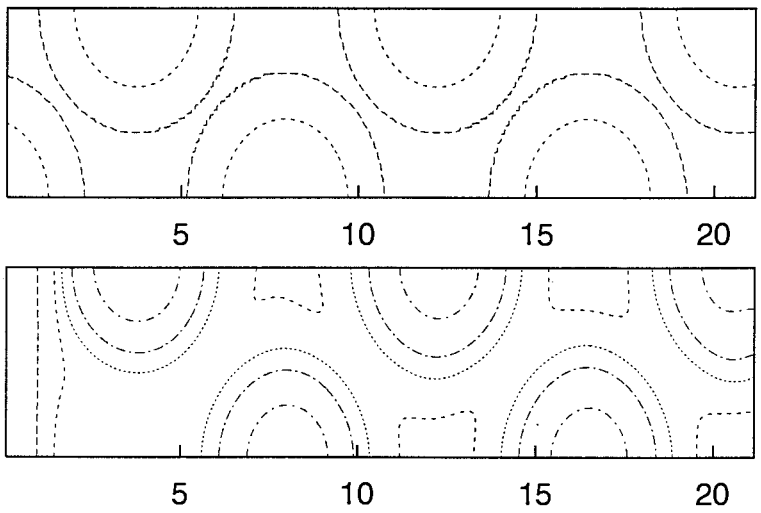

Figure 7. Contour plots of the gravure (top) and coating surface (bottom). Diamond pattern; time = 25. Contour levels for the gravure are −0·5 and −0·001; for the coating surface, they are −0·5, −0·2, 0, 0·2, 1.

that almost steady-state conditions have been achieved. The calculated fill fraction reaches about 44%.

In Figure 6, the fill fraction of cell (−1) is plotted *vs.* time for the three patterns, where an expanded scale has been used for clarity. The initial removal is virtually identical for all three. The minimum liquid volume in each cell is 42·7%. There is a degree of re-filling, however, as a portion of the liquid remaining on the land drains back into the cells. This re-filling is more pronounced for the hexagonal pattern. We note that the hexagonal pattern has a greater density of cells per unit area on the land than either of the other two patterns. Thus the cells are closer to one another. This may make them more prone to refilling.

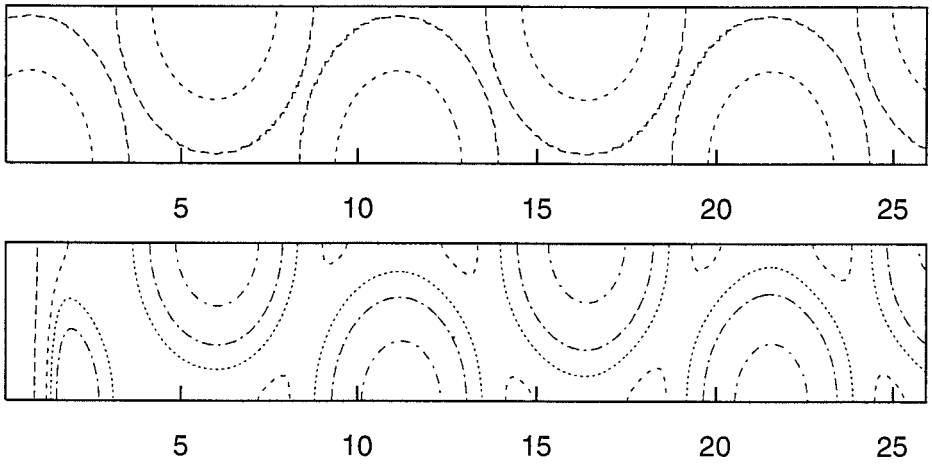

Figure 8. Contour plots of the gravure (top) and coating surface (bottom). Hexagonal pattern; time = 32. Contour levels for the gravure are −0·5 and −0·001; for the surface, they are −0·5, −0·2 ,0, 0·2, 1.

In Figures 7 and 8, contour plots of the gravure shape and free surface are shown for the diamond and hexagonal patterns, respectively. Each set of plots was taken near the end of the run when the time is about 20 per cent greater than that required for the pattern to traverse the length of the computational window; thus $t = 5b$. Note that a significant volume of liquid, with depth exceeding $0{\cdot}2h_0$, remains on the land area. This is the source of liquid that is available for refilling. The action of surface tension, which tends to minimize liquid-air interfacial area, is the driving force for refilling.

Figure 9 shows edge views of the liquid surface and the gravured substrate. Because the computational window is only one cell deep (in the y-direction) it gives a good picture of the menisci within the cells as well as showing the significant amount of liquid above the land level. The refilling of the cells with distance is also apparent, as the menisci within the cells are seen to rise, with increasing horizontal distance x, in each case.

4. Concluding remarks

We have continued development of a mathematical model to describe cell emptying in direct gravure-roll coating. Several different periodic patterns of cells have been considered. We find, perhaps surprisingly, that the initial removal, as the receding meniscus 'scrapes out' the cells, is quite independent of pattern. The pattern influence is restricted to the refilling process, with the hexagonal pattern, for which the cells are more closely packed, suffering a greater degree of refilling.

Only one particular cell shape and cell size has been investigated. Further investigation can reveal other valuable information. More complex rheology can be considered to ascertain whether there is a significant coupling between rheology and cell patterns. It is also a straightforward matter to generalize the procedure to consider other axisymmetric hole shapes; a suitable family is

$$h_1(r) = -h_0\left(1 - \frac{r^n}{r_0^n}\right), \tag{10}$$

where $n \geq 1$ for example. As n becomes large, the cells will be more nearly flat-bottomed.

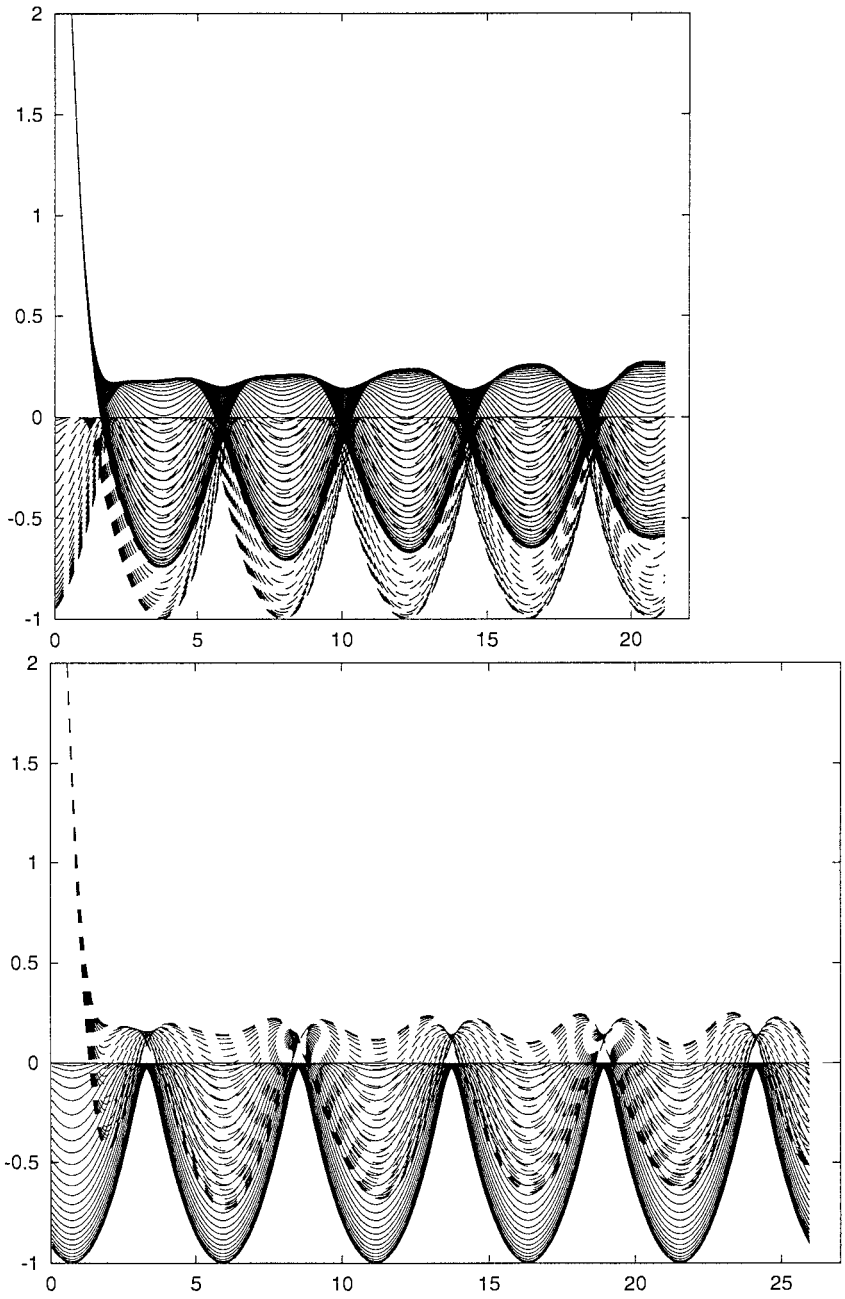

Figure 9. Edge views of the gravure and the coating. Top: diamond pattern, time = 25. Bottom: Hexagonal pattern, time = 32. Note the rise in meniscus height within the cells as one moves to the right. This indicates refilling.

Compared with actual experimental measures of cell emptying, the removed amounts reported here are somewhat large [5]. The most important determinants of cell emptying are cell size and meniscus curvature, the latter being expressed here by the prescription of meniscus slope. The large-removal conditions used here were chosen so as to illustrate more clearly the differences arising from the choice of cell pattern. In our previous work we used cells that were trapezoidal volumes, usually termed *quadrangular* in the coating literature [4]. Investigation

of these shapes, in various patterns, is another possible extension. It is quite likely to be true, however, that in actual operation, solidification of residual liquids in these sharp-cornered cells, may make the effective shape of the cells more like the paraboloidal shapes used here.

There are other types of gravure patterns that do not employ isolated cells. We have not yet considered trihelical patterns, *i.e.* triangular grooves that wind around the roller. We expect that emptying will be more complete, compared with the isolated cells considered here. Three-dimensional effects lead to a significant increase in the predicted residual liquid fractions compared to two-dimensional grooves. The reason for this is that the liquid surface, above a partially-filled isolated cell, is 'supported' on all four sides by the cell side walls in three dimensions. It is therefore more difficult to empty a cell because of the greater amount of working against surface tension. In previous work [4] grooves parallel to the roller axis were considered and they emptied more completely, as expected. In order to consider trihelical patterns, it will be necessary to change the boundary conditions on the sides of the computational window. In particular, the reflection-symmetry condition used here will need to be replaced by a periodic boundary condition. The lateral window size a will then be selected to match the pitch of the helix, in a manner consistent with the periodic boundary conditions.

5. Acknowledgements

This work was supported by ICI, The State of Delaware, and the NASA Microgravity Program.

References

1. F. Shepherd, *Modern Coating Technology Systems.* Barnet, U.K.: Emap Maclaren Ltd (1995) 156 pp.
2. V. G. Levich, *Physiochemical Hydrodynamics.* Englewood Cliffs: Prentice-Hall, (1962) 700 pp.
3. S. D. R. Wilson, The drag-out problem in film coating theory. *J. Eng. Math.* 16 (1982) 209–221.
4. L. W. Schwartz, P. Moussalli, P. Campbell and R. R. Eley, Numerical modeling of liquid withdrawal from gravure cavities in coating operations. *Chem. Eng. Res. & Design Trans. Inst. Chem. Engrs.* 76 (1998) 22–29.
5. H. Benkreira and R. Patel, Direct gravure roll coating operations. *Chem. Eng. Sci.* 48 (1993) 2329–2335.
6. C. A. Powell, M. D. Savage and P. H. Gaskell, Modelling the meniscus evacuation problem in direct gravure coating. *Chem. Engrg. Res. & Design Trans. Inst. Chem. Engrs.* 78 (2000) 61–67.
7. D. J. Benney, Long waves on liquid films. *J. Math. Phys.* 45 (1966) 150–155.
8. R. W. Atherton and G. M. Homsy, On the derivation of evolution equations for interfacial waves. *Chem. Eng. Comm.* 2 (1976) 57–77.
9. J. S. Kim, S. Kim and F. Ma, Topographic effect of surface roughness on thin-film flow. *J. Appl. Phys.* 73 (1993) 422–428.
10. M. D. Savage, Mathematical models for coating processes. *J. Fluid Mech.* 117 (1982) 443–455.
11. D. J. Coyle, C. W. Macosko and L. E. Scriven, Stability of symmetric film-splitting between counter-rotating cylinders. *J. Fluid Mech.* 216 (1990) 437–458.
12. L. W. Schwartz and R. R. Eley, Simulation of droplet motion on low-energy and heterogeneous surfaces. *J. Colloid Interf. Sci.* 202 (1998) 173–188.
13. M. H. Eres, L. W. Schwartz and R. V. Roy, Fingering phenomena for driven coating films. *Phys. Fluids* 12 (2000) 1278–1295.
14. D. W. Peaceman and H. H. Rachford, The numerical solution of parabolic and elliptic differential equations. *SIAM Journal* 3 (1955) 28–41.